TR - H - 179

Acoustic characteristics of the human paranasal sinuses derived from sound pressure measurement and morphological observation

Jianwu Dang Kiyoshi Honda

1995. 12. 11

ATR人間情報通信研究所

〒619-02　京都府相楽郡精華町光台2-2　☎ 0774-95-1011

ATR Human Information Processing Research Laboratories
2-2, Hikaridai, Seika-cho, Soraku-gun, Kyoto 619-02 Japan
Telephone: +81-774-95-1011
Facsimile: +81-774-95-1008

Acoustic characteristics of the human paranasal sinuses derived from sound pressure measurement and morphological observation

Jianwu DANG and Kiyoshi HONDA
ATR Human Information Processing Research Labs.,
2-2 Hikaridai Seikacho Soraku-gun, Kyoto, 619-02 Japan

ABSTRACT

This paper reports on the acoustic characteristics of the human paranasal sinuses as determined from sound pressure measurement and morphological examination. A new method has been developed in order to explore the anti-resonance patterns of an acoustic tract with a complex shape. This method uses a series of sound pressure measurements at two points: one is at the radiating end and the other moves along the acoustic tract. Spectral and spatial information obtained by the method enables us to acquire frequency and topological details of multiple anti-resonators within the tract. By applying this method to the nasal tract, the resonance frequencies of the paranasal sinuses and locations of their openings were obtained for three subjects, and the locations were used to correlate the resonance frequencies with the corresponding sinuses via the subjects' volumetric MRI data. The accuracy of the method is approximately 10% error, as determined by comparing measured values with numerical results obtained from the morphological data. The results from the experiments indicated that each of the three major sinuses, the sphenoidal, maxillary, and frontal sinuses, contributes its own zeros to the transmission characteristics of the nasal tract. Further, the anti-resonance patterns of the sinuses demonstrate strong individual differences and left-right asymmetry. On the basis of the acoustic and morphological data, the paranasal sinuses were modeled by a set of Helmholtz resonators to produce realistic nasal spectra. It was concluded that the paranasal sinuses not only cause spectral complexity but also shape the nasal formants.

PACS number: 43.70.Bk, 43.70.Aj, 43.72.Ct

INTRODUCTION

The paranasal sinuses are bilateral sets of airy cavities in the facial cranium, and each sinus is connected to the nasal cavity via a small opening, i.e., the ostium. Anatomically, they consist of four kinds of sinuses: the maxillary, sphenoidal, frontal, and ethomoidal sinuses, in which the former three have a left-right pair of cavities. It is widely believed that mammals' paranasal sinuses play a role in the olfactory function of the nose. In humans, however, the role of the sinuses is mysterious as repeatedly noted in the literature (c.f. Koyama, 1966; Lindqvist-Gauffin and Sundberg, 1976; Takeuchi, et al., 1977; Lang, 1989; Donald, 1995). Surgical alteration of their structure causes no evident disadvantage to the quality of our life, supporting the idea that they help reduce the weight of the cranium (Davies, 1967). The explanations in the literature also refer to their role in the speech function, e.g., adding resonance to the voice. By their morphological characteristics, the sinuses must contribute constant, significant acoustic effects to human nasal sounds, but these accounts lack experimentally-tested causal relationships.

The study of nasal and nasalized sounds has been a crucial and long-standing issue. So far, two different approaches have been used to investigate the acoustic characteristics of the nasal and paranasal cavities: one is to focus on acoustical cues of nasal sounds (c.f. Hattori, Yamamoto, & Fujimura, 1956; Maeda, 1982), and the other is to begin with the morphology of the nasal and paranasal cavities (c.f. House and Stevens, 1956; Fant, 1960). In past studies, House & Stevens (1956) and Fant (1960) proposed area functions of the nasal tract, which were obtained from a cadaver specimen and a plastic mold of the nasal tract, respectively. Using his area function, Fant (1960) interpreted spectral changes in nasalization spectra in terms of the degree of coupling between the oral and nasal cavities.

It has been pointed out, however, that those morphological data do not adequately account for the characteristics of naturally observed nasal

sounds (Fujimura & Lindqvist, 1971; Takeuchi, Kasuya & Kido, 1977; Maeda, 1982). Results from sweep-tone experiments (Fujimura & Lindqvist, 1971) have shown that the locus of nasal pole-zero pairs is close to or often below the first formant peak, especially for low vowels, while the pole-zero pair predicted from traditional models (without the paranasal cavities) is located above the first vowel formant peak. These facts have suggested that the acoustic effect of the paranasal sinuses and/or of the asymmetry of the nasal passages may play a significant role in forming reasonable nasal spectra (Fujimura & Lindqvist, 1964; Fant, 1980). To solve the discrepancy, Maeda (1982) introduced a cavity corresponding to the maxillary sinus into his nasal model, and synthesized nasal and nasalized vowels by changing the parameters of this cavity. He reported that appropriate nasal formants can be obtained when the anti-resonance frequency of the cavity is adjusted to about 450 Hz.

On the other hand, several studies have tried to reveal acoustical contributions of the paranasal sinuses by means of experiments. Among them, Koyama (1966) estimated the anti-resonance frequencies of the sphenoidal and maxillary sinuses through acoustic measurements on a model of the nose. Further, he analyzed nasal sounds recorded under normal conditions and while obstructing the ostia of the maxillary sinus for eight living subjects. The frequencies of spectral valleys were observed to change by 400 to 1000 Hz for the subjects.

Lindqvist-Gauffin and Sundberg (1976) used a probe sound source to excite the nasal cavity, and recorded nasal sounds under the condition of a closed velum. They concluded that the zeros remaining stationary during movements of the sound source were caused by the paranasal sinuses. Their simulation with a nasal cavity model suggested that anti-resonance frequencies ranged from 200 to 800 Hz for the maxillary sinus, and from 500 to 2,000 Hz for the frontal sinus.

Takeuchi et al. (1977) studied the cause of the differences between synthetic and real nasal sounds, and noted that the paranasal sinuses may be the cause of the differences. They measured the cavity volume and the ostium size of a cadaver specimen for the sphenoidal, maxillary and frontal

sinuses. Anti-resonance frequencies of the paranasal sinuses were estimated, where the sinuses were considered to be symmetric between the left and right sides. They found that when the sinuses were included in the nasal model, zeros appeared in the range of 400 to 500 Hz for the maxillary sinus, at approximately 1 kHz for the frontal sinus, and at approximately 1.5 kHz for the sphenoidal sinus.

Masuda (1992) focused on the role of the maxillary sinus as a resonant cavity, and measured the maxillary sinus by dissecting more than 20 skulls. He also observed changes of the valleys in nasal spectra when obstructing the opening of the ostia for 13 living subjects. He indicated that the anti-resonance frequencies of the maxillary sinus ranged from 1 to 2 kHz and varied considerably among individuals.

These results reported in previous studies on the paranasal sinuses are summarized in Table I. As shown in this table, their conclusions are sometimes quite different. For example, the anti-resonance frequency range for the maxillary sinus was reported to be 400 to 1000 Hz by Koyama (1966), but 1000 to 2,000 Hz by Masuda (1992). Such differences may be induced by instrumental problems such as the lack of mucosa in the cadaver specimen, or inadequate assumptions in the analysis which conflict with the real morphology of the paranasal cavities.

The authors examined the three-dimensional geometry of the nasal and paranasal cavities using the MRI technique (1994) and investigated their acoustical properties for living subjects (1995a). Acoustic simulation using our area function of the nasal tract resulted in realistic nasal formants. Further, the simulation with the paranasal sinuses showed that these cavities must be taken into account in establishing an accurate production model of nasal sounds. Unfortunately, precise measurement of the dimension of the ostia of the paranasal sinuses is difficult, since their size is close to the resolution limit of the current MRI technique. For the above reasons, observations from more deliberate methods are required for exploring the acoustical properties of the paranasal sinuses.

The present study proposes a new method for revealing detailed vocal tract transmission characteristics. The proposed method is applied to investigate the acoustic characteristics of the paranasal cavities with the aid of MRI-based morphological clues. The complexity of the paranasal sinuses is represented as a "four-zeros model" on the basis of acoustic and morphological data.

I. METHOD

The proposed method uses two sound pressures, which are measured simultaneously at two points: one within an acoustic tract and one at its radiating end, to determine the transmission characteristics between the two points. A series of transmission characteristics for the tract segments is obtained by repetitive measurements while exciting the tract at the glottis and moving the inner pressure transducer along the tract. The array of the transmission functions infers characteristic frequencies of the resonators and information on the locations of the resonators' openings if branch resonators exist in the tract segments. The nature of the transmission functions is utilized in our method. This section describes the theoretical consideration and experimental verification of the method.

A. Theory

Sound waves can be approximately considered to propagate in one dimension in an acoustical tube when the cross-sectional dimension of the tube is appreciably smaller than the wavelength. For the vocal tract, sound waves can be approximated by a plane wave for the frequencies below about 4 kHz. With this assumption, the vocal tract is represented by a cascade concatenation of small sections. On the basis of the transmission line theory, a general chain matrix of a portion of the tract relates output pressure P_O and volume velocity U_O to the input pressure P_I and volume velocity U_I (capitalized in order to denote variables in the frequency domain). Thus,

$$\begin{bmatrix} P_o \\ U_o \end{bmatrix} = \begin{bmatrix} A & B \\ C & D \end{bmatrix} \begin{bmatrix} P_i \\ U_i \end{bmatrix} = M \begin{bmatrix} P_i \\ U_i \end{bmatrix} \qquad (1)$$

where the input is the glottal side, and the output side is toward the lips and nostrils. Sondhi and Schroeter (1987) gave expressions to include distributed vocal tract losses in the matrix; these losses are produced by mucous friction, heat conduction and wall vibration. Thus, transmission characteristics of the vocal tract can be represented by a multiplication of several chain matrices.

For convenience, an acoustic tube with a branch is used to explain the proposed method. A diagram of the acoustic tube is shown in Fig. 1. There, we aim at a tube segment from a selected point x_i to the radiating end x_e of the tube. The selected point x_i is referred to as the input point of the tube segment. The branch is located at position x_b in the tube segment. The transmission characteristics are represented for the tube segment from the input point to the radiating end of the tube using three matrices in the following equations.

$$\begin{bmatrix} P_r \\ U_r \end{bmatrix} = K_1 K_b K_2 \begin{bmatrix} P_i \\ U_i \end{bmatrix} \tag{2}$$

$$K_1 = \begin{bmatrix} A_1 & B_1 \\ C_1 & D_1 \end{bmatrix},\ K_2 = \begin{bmatrix} A_2 & B_2 \\ C_2 & D_2 \end{bmatrix},\ K_b = \begin{bmatrix} 1 & 0 \\ -Y_b & 1 \end{bmatrix} \tag{3}$$

where P_r and U_r denote the pressure and volume velocity at the radiating end. P_i and U_i are the pressure and velocity at the input point. K_1 depends on the tube segment from the branch location x_b to the radiating end x_e. K_2 is the chain matrix corresponding to the part from the input point x_i to the branch location x_b. For a tube segment that includes a side branch, a special coupling matrix is needed for computing the chain matrices. K_b is the coupling matrix of the side branch, where Y_b denotes the input admittance of the branch.

In exploring the acoustic properties of an acoustic tract, a few different kinds of transfer functions, such as velocity-to-velocity and pressure-to-pressure transfer functions, are usually employed. Velocity-to-velocity and pressure-to-pressure transfer functions contain the same information on anti-resonances, though they demonstrate different sets of peak patterns. It is known, however, that accurate measurement of the

volume velocity is difficult at low frequencies when the excitation source has a small acoustic power. For this reason, pressure-to-pressure transmission characteristics were adopted in this study. By computing the ratio of the output sound pressure to the input pressure of Eq. (2), the transmission characteristic T of the tube segment from the input point to the radiating end is given by

$$T = \frac{P_r}{P_i} = \frac{Z_r}{B_2(Z_rC_1 - A_1) + D_2(Z_rD_1 - B_1) - Y_bB_2(Z_rD_1 - B_1)} \qquad (4)$$

where Zr is the radiation impedance at the radiating end. Note that all of the terms on the right side of Eq. (4) are dependent only on the geometry of the tube segment from the input point to the radiating end. In other words, the transmission characteristics obtained from Eq. (4) are independent of the tube segment behind the input point (i.e., the portion from the source to the input point). Equation (4) indicates that zeros appear in the transmission characteristic at the frequencies where the input admittance Y_b is infinite as long as $B_1 - Z_rD_1 \neq 0$. That is, the zero pattern (i.e., the distribution of the zeros disregarding changes in the peaks) of the transmission characteristic does not vary even if the input point is moved in the region behind the location of the branch. When the input point is moved in front of the location of the branch, Equation (4) reduces to

$$T = \frac{P_r}{P_i} = \frac{Z_r}{Z_rD_1 - B_1} \qquad (5)$$

Equation (5) shows that the zeros disappear from the transmission characteristics when the branch is excluded from the tube segment.

When the input point moves along the acoustic tract, as described above, the zero pattern of the transmission characteristics from the input point to the radiating end varies only when the input point passes through the location of the branch. This behavior correlates a zero pattern to a branch. Thus, the details of anti-resonators can be acquired by means of a series of transmission characteristics from a set of the input points to the radiating end. The location of a branch is inferred by spatial information

(i.e., variations of the zero patterns with the input point), and the anti-resonance frequency of the branch is determined by the appearance or disappearance of the zeros when the input point passes through its location.

B. Experimental verification

A pilot experiment was conducted to verify the validity of the proposed method by applying the method to acoustic tubes of known geometries. The accuracy was evaluated by measuring resonances and anti-resonances in transmission characteristics and detecting the location information of the branch. A schematic diagram of the experimental setup is shown in Fig. 2. In the experiment, a sweeptone signal was generated using a function generator, FG-143 (NF Circuit Design Block Co.). A horn driver unit, SG-505FRP (Goto Unit Co.), was used to feed the source sound into the test tubes. The joint between the acoustic tube and the throat of the horn driver was sealed with plasticine to prevent sound leakage. Two microphones were used to record sound pressures inside and outside the acoustic tube. Microphone M1, a B&K-4003, was placed about 6 cm away from the radiating end of the tube to record the radiation sound pressure. Probe microphone M2, a B&K-4182, was used to measure the sound pressure inside the tube via a flexible probe tube. The probe tube with a matched impedance to the microphone had an outer diameter of 0.165 cm and an inner diameter of 0.076 cm. Note that the location of the tip of the probe tube is referred to as the measurement point. The segment from the measurement point to the radiating end of an acoustic tube is called the measurement segment.

Signal recording was carried out at a sampling rate of 44.1 kHz in an anechoic room. The temperature was kept at 20°C during the measurement, so the sound velocity was assumed to be approximately 34,300 cm/s. The frequency range of the sweeptone signal was from 100 to 7,500 Hz with a sweep period of 100 ms. An FFT-derived cepstrum analysis (Imai & Abe, 1979) was applied to the pressure signals in order to obtain the envelope of the spectra; the cepstrum coefficients were weighted by a Hamming window with a length of 1.2 times the fundamental period of the signals.

Numerical values for the transmission characteristics were calculated using the transmission line model of Eqs. (4) and (5). The radiation impedance was approximated by a cascade connection of radiation resistance and radiation inductance (Cassé et al., 1984), which is a valid model as long as $kr < 1.5$, where k is the wave number and r is the radius of the radiating end. Losses of viscous friction and heat conduction were implemented into the computation (Flanagan, 1972). The end correction length for the branches was approximately 0.8 times the radius of the radiating end (Fant, 1960).

C. Accuracy of the proposed method

Three stiff plastic tubes were employed as the test acoustic tubes in this verification. The tube wall was assumed to be non-yielding. The geometries of the acoustic tubes are given in Table II. The tubes had a uniform circular cross-section with different branching configurations. Data recording was repeated while the measurement segment was increased in 1-cm intervals. The cross-sectional dimension of the tubes enables us to use the plane-wave model to discuss their frequency characteristics up to 6 kHz.

Measurements of transmission characteristics were performed on the measurement segments from 4 to 18 cm for both Tube A and Tube B. The results are shown in Fig. 3. The lengths of the measurement segments are shown on the right side of each panel. Figure 3(a) shows the results obtained from a uniform tube, Tube A, for each measurement segment. As expected, with increasing length of the measurement segments, the frequencies of the peaks decrease monotonically, and the number of peaks increases in the frequency range from 0 to 6 kHz. Some spectral irregularities can be seen in the low frequency region below 100 Hz. This is because the excitation source of the sweeptone signal had no power in this region.

The accuracy of the method was evaluated on the basis of comparisons between computed and measured values for the resonance frequencies and their bandwidths. The relative difference of frequencies

(RDF) of the peaks, i.e., the ratio of errors between the measured and computed values to the computed values for resonance frequencies, was within 2% for all of the measurement segments. For the bandwidths, the measured values were about 40% wider than the computed values in the region below 2 kHz. Errors of the bandwidth were smaller, within 10%, in the region above 2 kHz. There are two possible reasons for the errors in the low frequency region. One is that the scan period of the sweeptone signal was not long enough to define the sharpness of the peaks for the tube. The other reason is that the wall of the acoustic tube may not have been completely rigid in this frequency range.

A complex tube, Tube B, was employed for verifying the validity of the method. The results are shown in Fig. 3(b). In contrast to the results of the uniform tube shown in Fig. 3(a), there are a number of zeros in the transmission characteristics for this tube. The zeros with a constant interval, indicated by the dashed lines, appear in the spectral curves of the measurement segments of 6 cm and longer. At 12 cm, a variation of the zero pattern is recognized at a frequency just above 2 kHz, as indicated by the arrow. This can be judged as another zero pattern caused by a different branch within the tube, since it also appears consistently in the results for the measurement segments longer than 12 cm. Thus, the results in Fig. 3(b) lead us to believe that this acoustic tube has two branches: one is located about 6 cm from the radiating end; the other one is located about 12 cm back from the radiating end. These two zero patterns have different first anti-resonance frequencies, and it is reasonably inferred that the former branch is longer than the latter one. These estimations are consistent with the geometrical data shown in Table II for Tube B. As described in the theoretical considerations, variations of zero patterns with the measurement point indicate the locations of branches in a tube. Spectral patterns were obtained by applying the transmission line model to the geometrical data, and they were found to be almost identical to the measured data. A comparison of the measured and numerical values showed that the RDFs of the zeros were smaller than 2% for the longer branch, and about 3% for the shorter branch. The RDFs of the peaks were

about 3% for measurement segments shorter than 6 cm, and about 5% for measurement segments of 6 cm and longer.

The validity of the method was also verified using speech sound as the excitation source, where the subjects kept one end of the tubes attached to their mouth and produced a steady-state vowel /o/ (Dang & Honda, 1995b). The same accuracy as that described above was obtained for the frequencies of the resonances and the anti-resonances. This fact insures that the method is applicable for detailed estimation of vocal tract transmission characteristics from short-period data of natural utterances.

The results of the experiment indicate that this method is capable of estimating spectral and geometrical details of side branches in a complex acoustic tube by means of the successive measurement of transmission characteristics along the tract. Due to the nature of the spatial domain, the accuracy of the method is preserved even if the anti-resonance frequencies of the branches are close to each other.

II. MORPHOLOGY OF THE PARANASAL SINUSES

Our proposed method uses spatial analysis of zero patterns and information of the location of sinus opening to infer the relationship between observed anti-resonance frequencies and the paranasal sinuses producing them. Therefore, morphological information plays a critical role in the interpretation of anti-resonance of the sinuses, and it is of benefit to describe the morphology of the nasal and paranasal cavities. This section provides a brief anatomical description and a morphological description for the subjects which was obtained from MRI recordings.

Figure 4 depicts the relevant structure in two displays: (a) a projection of 3D image of the nasal airway with all the paranasal sinuses, and (b) a sagittal view of the three major sinuses and their ostium openings. The 3D image in Fig. 4 (a) was reconstructed from cross-sectional MRI images in the coronal plane (Dang, et al., 1994), and it shows a gross image of the paranasal sinuses attached to the nasal cavity. The paranasal sinuses consist of four anatomical groups: the sphenoidal sinus (S. S.), the maxillary sinus (M. S.), the frontal sinus (F. S.) and the

ethomoidal sinus (E. S.). The former three sinuses normally have a left-right pair of cavities; each cavity is adequately represented by a Helmholtz resonator. On the contrary, the ethomoidal sinus is composed of many small cells, and its acoustic characteristics are not simply modeled by a few lumped parameters. However, the fine cellular structure of the ethomoidal sinus is judged not to contribute to the acoustic characteristics of the nasal sounds in the frequency region below 3 kHz (Koyama, 1966; Takeuchi, et al., 1971). In accordance with these reports, the present study focuses on the other three major sinuses, and examines their frequency characteristics in the region below 3 kHz.

Since the paranasal sinuses develop as pneumatizations of solid bones, the extent of this process is variable between sides as well as across individuals (Dang, et al., 1994; Donald, 1995). According to the authors' experience on measuring the sinus structure, image resolution of the MRI technique limits the accuracy of ostium dimensions that are critical to the anti-resonance frequencies of the sinuses. Therefore, we refer to the anatomical literature by Lang (1989) and by Donald (1995) to obtain the canonical values for the three major sinuses that are shown in Fig. 4 (b).

The sphenoidal sinus is a usually paired and asymmetrically developed pneumatization of the body of the sphenoidal bone. The openings of the sinus, which are called either a "duct" (if it is longer usually than 3 mm) or an "ostium" (if shorter), are usually located in the upper one-third of the anterior wall of the sphenoidal sinus. The ostium was round in the majority of specimens examined by Lang and averaged 0.34 cm in diameter (Lang, 1989). The length of the ostia was around 0.3 cm (Donald, 1995).

The maxillary sinus is the end result of the pneumatization of the maxillary bone. Two cavities of the sinus are bilaterally located in the left and right sides of the nasal tract. The majority of the sinus openings are located from the posterior to the middle parts of the lateral wall of the middle nasal meatus. These openings are round or oval in shape for most healthy individuals (Donald, 1995). Most of the openings are the ducts, i.e., the lengths are longer than 0.3 cm. The average values for the opening

diameter are 0.24 and 0.44 cm in female and male cases. The anatomical data for Japanese examined by Masuda (1992) were 0.46 cm for diameter and 0.25 cm for length on the average. The maxillary sinus often has an additional opening, an "accessory ostium," in about 30% of the cases (Lang, 1989). This ostium is usually a small hole in the thin membrane that cover natural bony dehiscences in the middle meatus called fontalnelles, whose diameters were 0.22 and 0.34 cm on the average in female and male cases (Lang, 1989).

The frontal sinus is a pneumatization of the frontal bone that originates either by the development of a frontoethmoidal air cell that invades the frontal bone or as an upward extension of the infundibulum of the middle meatus of the lateral nasal wall. The ducts of the frontal sinus lead from the anteromedial extent of the each cavity into the infundibulum of the middle meatus respectively. The duct width averages 0.51 cm at its widest and 0.2 to 0.6 cm at its most narrow. The length of the duct averaged 0.62 cm, with a range of 0.32 to 1.49 cm (Donald, 1995).

The above anatomical data provide average values for the morphology of the sinuses, while the individual variation of the ostium dimensions is only represented by statistical summaries of their widths and heights, and so on. Fortunately, volumetric MRI data are available to infer the volumes of the paranasal cavities and the locations of their openings with the anatomical index of the individuals. The subjects who participated in this study had also served in our previous MRI study (Dang et al., 1994). For the purpose of the present study, the original MRI data were re-examined and the necessary information was summarized in Table III. The ostium location is shown by a linear distance between the vertical projection of the opening on the nasal floor and the outlet of the nostrils on the nasal floor. To summarize the table, the sphenoidal sinus has its ostia most posteriorly among the major sinuses, and the frontal sinus has the duct opening most anteriorly. This order of the ostium locations in the nasal cavity appears to be anatomically invariant across speakers. Note that all the ostium openings are located in front of the posterior nares. This situation permits our acoustic measurements on each side of

the nasal cavity separately without obvious interference form the other side.

It should be noted that MRI images do not normally show clear details for the ducts of the frontal sinus. Accordingly, the accuracy for this measurement is limited. Contrarily, the ostia of the maxillary and sphenoidal sinuses are almost always identifiable. Subject 3 showed a different shape of the maxillary sinus from the others, since he had received an operation on the sinus bilaterally (Caldwell-Luc operation). The maxillary sinus of this subject has an enlarged ostium and a surgical opening to the inferior nasal meatus.

III. EXPERIMENTAL PROCEDURE

According to the experimental verification and morphological analysis, the proposed method has been proved to be capable of identifying the zeros of nasal tract transmission characteristics with their corresponding paranasal sinuses. This section describes the procedures of sound pressure measurement and data analysis.

A. Experimental setup

The experimental setup for measuring the sound pressures in the nasal tract and at the radiating end of the nostrils is shown in Fig. 5. Microphone M1, a B&K4003, was placed 15 cm from the lips to record radiated sound pressures. Probe microphone M2, a B&K4182, was used to record sound pressures inside the nasal tract via a 30-cm-long flexible tube. The flexible tube with a matched impedance to the microphone had a 0.165-cm outer diameter and a 0.076-cm inner diameter.

Unlike in the pilot experiment, a few precautions were needed for recording pressure signals in the nasal cavity of living humans. When the flexible probe tube was inserted into the nasal cavity, the tip of the fine tube could be placed in contact with the nasal mucosa. Such a situation could interfere with correct pressure recording and often caused clogging of the tube with the mucus lining of the nasal mucosa. To prevent this event, a small vinyl balloon with a 0.6 cm diameter (marked B

in Fig. 5) was attached to the probe tube near the tip for isolation from the mucosa. The microphone signals were continuously monitored on an oscilloscope screen throughout the experiments so that when the mucous clogging occurred it could be removed by injecting air into the tube.

B. Data recording and analysis

The experiment was conducted on three subjects in an anechoic room. The speech materials shown in Table IV included 10 Japanese NV syllables and two isolated nasal consonants. The nasal cavity of each subject was treated with topical anesthetics (lidocain, 4%) and nasal decongestant (naphazoline HCl, 0.05%). The flexible tube of the probe microphone was inserted along the floor of a side of the nasal passages into the nasopharynx about 8 cm posterior from the nostrils. To ensure sound radiation from the corresponding side of the measurement, the other side of the nares was blocked by the finger during the measurement. Digital recordings were made at a sampling rate of 44.1 kHz. The measurement segment was decreased from 8 to 4 cm by a 0.5-cm interval. Each subject uttered the speech materials 36 times: two times for each measurement segment length on each nasal passage. At each session for the measurement segments, the subjects ware instructed to prolong production of the nasal consonant in the NV syllables.

A stable period in nasal consonants was selected from each sample for spectral analysis. The spectral pattern for each sample was obtained by averaged FFT power spectra with a 4096-point frame and a 1024-point shift-length. An FFT-derived cepstrum analysis (Imai & Abe, 1979) was applied to the pressure signals in order to obtain the envelope of the spectra, where the cepstrum coefficients were weighted by a Hamming window of 1.2 times the fundamental period of the signals. The results from the nasal consonants /m/ and /n/ were averaged in the final results, since the nasal tract geometry is thought to be invariant across these consonants.

IV RESULTS OF ESTIMATION OF ANTI-RESONANCE

On the basis of the theoretical considerations described in Section I, experiments were performed on both the left and right sides of the nasal

passages for the three subjects. Pressure signals were recorded for the series of measurement segments (MSGs) from 4 to 8 cm with 0.5-cm intervals. Spectral patterns were obtained for all the measurement segments and are shown in the arrays in Fig. 6 - 8. Two procedures were used to estimate the anti-resonance characteristics of the paranasal cavities: 1) estimation of branch locations from variations in zero patterns of the transmission characteristics for a series of measurement segments, and 2) identification of anti-resonance frequencies with corresponding paranasal sinuses by matching the estimated locations with real locations of the ostium openings for each of the paranasal sinuses.

Figure 6 shows the transmission characteristics obtained from the MSGs for Subject 1: (a) for the left nasal passage and (b) for the right side. The length of the measurement segment is shown on the right side of each panel, which also is the distance from the nostrils to the tip of the probe tube. As expected, longer measurement segments have more complex zero patterns since more sinuses are included in the segments.

As Fig. 6 (a) shows, there are three zeros in the frequency region below 2 kHz, which appear consistently in longer MSGs at about 630, 1100, and 1350 Hz. The zero at 1350 Hz, shown by the V-shaped arrows, appears in the transmission characteristics obtained in the MSGs from 8 to 6.5 cm, and disappears from the MSGs of 6 cm and shorter. This variation in the zero patterns implies that a branch, which induces the zero of 1350 Hz, is located between 6 and 6.5 cm. The MRI data shown in Table III indicate that the opening of the sphenoidal sinus was located 6.2 cm back from the nostrils for this subject. With reference to the morphological data, therefore, the branch is uniquely judged to be the sphenoidal sinus, and the zero of 1350 Hz is determined to be the anti-resonance frequency of the sphenoidal sinus.

Similarly, the zero at about 1100 Hz, indicated by the black arrows, appears in the spectra for the MSGs of 5.5 cm and longer, and disappears from the spectra for the MSGs of 5 cm and shorter. According to the morphological data, this zero is judged to be caused by the maxillary cavity. The other zero, shown by the white arrows, appears at about 630 Hz in the

spectra for all the MSGs longer than 4 cm, and disappears from the spectrum for 4 cm. These variations indicate that a branch exists in the region between 4 and 4.5 cm back from the nostrils. The MRI data listed in Table III show that the ostium opening of the frontal sinus is in this region. Thus, the results lead us to believe that the branch is the frontal sinus, and the zero is induced by this sinus.

Employing the same procedure, estimations were made based on the spectra for the right side of the nasal cavity, which are shown in Fig. 6(b). Anti-resonance frequencies of the paranasal sinuses are 750 Hz for the sphenoidal sinus, 890 Hz for the maxillary sinus, and 2060 Hz for the frontal sinus. A large difference caused by left-right asymmetry can be seen in the anti-resonance frequency for the frontal sinus.

Figure 7 illustrates the transmission characteristics of the measurement segments for Subject 2. For the left side of the nasal cavity shown in Fig. 7(a), the anti-resonance frequencies of the sphenoidal and maxillary sinuses are easily estimated from the variation of the zero patterns. The anti-resonance frequencies are approximately 1900 Hz for the sphenoidal sinus and 630 Hz for the maxillary sinus. In contrast, the effects of the frontal sinus are not clear in these patterns. The zero at 2360 Hz seems to be caused by the frontal sinus in terms of the spatial information, since the frontal sinus is located about 4 cm from the nostrils (see Table III) and the zero appears in nearly all of the MSGs 4 cm and longer, but it is not well-defined for MSGs of 7.5 and 8 cm. It is, however, difficult to believe that the zero frequency is induced by the frontal sinus because the value for the sinus cannot seem to be obtained from the MRI data of 4.9 cm^3 in volume for the subject with some appropriate cross-sectional areas and lengths given with reference to the anatomical data. For these reasons, it should be concluded that there is no zero caused by the frontal sinus, probably due to some mucosa clogging in its duct.

There are three zeros in the results from the right side of the nasal cavity shown in Fig 7(b). Two of them, at about 580 and 1450 Hz, appear in all MSGs (the zero at 1450 Hz does not appear in the MSG of 5 cm probably owing to an interaction with some resonance peaks.) Therefore, it is

difficult to determine which zero corresponds to the maxillary sinus. However, when this sinus is approximated to a Helmholtz resonator, an anti-resonance frequency on the order of 500 Hz is expected for the maxillary sinus from this subject's MRI data (see Table VI). Consequently, the zero at 580 Hz was considered to correspond to the maxillary sinus, and the remaining one was judged to belong to the frontal sinus.

The results for Subject 3 are shown in Fig. 8. The zero patterns in these results are more complex than those from the other subjects. In the lower part of each side, there are four zeros in the transmission characteristics below 2 kHz. In terms of the spatial analysis of the zero patterns, it is easily determined that the zero at 930 Hz is caused by the left and right cavities of the sphenoidal sinus, respectively. In Fig. 8(a), two zeros, at about 530 and 1160 Hz, appear in all spectral curves consistently. The morphological data in Table III also show that the opening locations were close to one another for the maxillary and frontal sinuses. From the subject's MRI data, it is difficult to find clear correspondence between the two zeros and the two cavities of the sinuses. It may be noticed that the zero at 1160 Hz becomes more conspicuous when the measurement point approaches the MSG of 4 cm, while the zero at 530 Hz gets slightly weaker. This suggests that the opening location corresponding to the zero at 530 Hz is posterior to the other. According to this suggestion, the zero at 530 Hz is produced by the maxillary sinus, and the zero at 1160 Hz is caused by the frontal sinus. In Fig. 8(a), a zero-like dip also appears at about 1400 Hz. It is difficult to give an appropriate explanation for the dip because its frequency increases monotonically with decreasing lengths of the measurement segment.

According to the spatial analysis of the results of Fig. 8(b), it can be easily deduced that the zero at about 1700 Hz is produced by the sphenoidal cavity. Besides the zero at 1700 Hz, there is a zero pair (400 and 510 Hz) and a zero at 740 Hz. The zero at 740 Hz becomes prominent while the zero pair gets weaker with decreasing MSGs. With reference to MRI data, this phenomenon can be explained in that the opening corresponding to the zero at 740 Hz is anterior to those corresponding to the zero pair. Therefore, the zero at 740 Hz is judged to be caused by the frontal sinus.

Since the subject had an operation on the paranasal cavity, the maxillary sinus had two openings to the main nasal passage. This fact can explain why the right maxillary cavity caused a pair of zeros.

The anti-resonance frequencies of the paranasal sinuses estimated above are shown in Table V for the three subjects. The ranges of the anti-resonances are from 750 to 1900 Hz for the sphenoidal sinus, from 400 to 1100 Hz for the maxillary sinus, and from 630 to 2060 Hz for the frontal sinus. The results show that the three main paranasal sinuses: the sphenoidal, maxillary and frontal sinuses, contribute zeros to the transmission characteristics of the nasal tract. Strong left-right asymmetry and large individual variations are observed in the anti-resonance frequencies of these paranasal cavities.

V. SIMULATION AND MODELING

The above results demonstrate that the paranasal sinuses introduce complex anti-resonance patterns in nasal tract transmission characteristics. This complexity indicates that a single-tube or a dual-tube model is not sufficient to account for the acoustic properties of the nasal tract, and suggests the necessity of including the paranasal sinuses in a realistic model of the nasal tract. To model the complexity, this section gives some reasonable simplifications, in which the paranasal sinuses are represented by a set of Helmholtz resonators. The accuracy of the simplification is verified by comparing the acoustical measurements and numerical results based on the morphological data.

A. Comparisons of the measured and computed resonance of the sinuses

A paranasal sinus is characterized by an airy cavity with a narrow throat, which forms a typical Helmholtz resonator. Its resonance frequency is determined by the volume of the cavity and the dimensions of the throat. The latter is specified by the diameter and the length of the throat. Assuming a lossless case, the resonance frequency is evaluated by the following formula:

$$f = \frac{c}{2\pi}\sqrt{\frac{A}{l_e V}} \qquad (6)$$

Where A and l_e are the cross-sectional area and effective length of the throat, respectively. V is the dimension of the volume.

To obtain a more realistic resonance bandwidth, it is necessary to include appropriate losses. With the viscous resistance R in the throat and the loss G caused by the wall vibration, the resonance frequency of a Helmholtz resonator is evaluated using the following formula (Fant, 1960):

$$f = \frac{c}{2\pi}\sqrt{\frac{1+RG}{LC} - \frac{1}{4}\left(\frac{R}{L}+\frac{G}{C}\right)^2} \qquad (7)$$

where $L = \rho l_e / A$ and $C = V / \rho c^2$.

In modeling the paranasal sinuses, only the viscous resistance of the throat and the wall vibration of the cavity are considered, since possible loss from heat dissipation is much smaller. The viscous resistance of the throat was evaluated using a well-known formula (see Flanagan, 1972, p.34). The wall vibration is usually represented by wall impedance including a resistive part and a mass reactive part, which depend on the cavity wall properties. Since the sinus wall consists of a bony wall with a thin layer of mucous membrane, it is approximately assumed that the mucous membrane is the only factor involved in the vibration. Since the density of the mucosa is about the same as that of water, the reactive mass can be evaluated from the thickness of the mucous layer. Our MRI data showed that the mucous layer on the inside surface of the paranasal cavities is much thinner than that of the main nasal passages, where the latter is about 0.2 cm thick on the average. However, the MRI data were not able to offer an exact value for the thickness. According to Donald (1995), sinus mucosa is quite uniform in thickness for each sinus: 0.02 to 0.07 cm in the frontal and sphenoidal sinuses and 0.03 to 0.08 cm in the maxillary sinus. To observe the effects of the mucosa, the mass per-unit-area was changed in a range from 0.02 to 0.2 g/cm^2 in this estimation. The resistive component was changed from 1500 to 8500 g/(s•cm^2). The values of the

resistive and mass reactive components of the wall impedance were justified to obtain a realistic bandwidth of the resonances. Under given conditions, the resonance frequencies increase about 6% and the bandwidths approximately double when the resistive component decreases from 8500 to 1500 g/(s•cm^2). With reference to our acoustic measurements in which the value of the bandwidth ranged from about 100 to 200 Hz for the sinuses, the resistive component was approximately equal to 6500 g/(s•cm^2) when the bandwidths become appropriate.

In contrast, increasing the mass reactive component showed a tendency to raise the resonance frequency and to narrow the bandwidth. However, the changes were only 0.5% in both the frequency and bandwidth when the mass varied from 0.02 to 0.2 g/cm^2. This shows that the mass reactive component of the wall is less sensitive in the lower frequency region we are interested in. With reference to both the numerical and morphological data, the value of the mass per-unit-area is reasonably defined to be 0.05 g/cm^2, which is the average value of Donald's data (1995). Thus, the wall impedance of the paranasal cavity is approximately

$$z_w = 6500 + j\omega 0.05 \qquad (8)$$

To evaluate the accuracy using the Helmholtz resonator to model the paranasal sinuses, a comparison was made between the acoustic measurements and numerical computations based on the morphological data. Since the image resolution is close to the size of the ostia, our MRI data have a limitation in estimating these morphological values. So far, reliable ostium dimensions were obtained for the maxillary sinus from volumetric MRI data for Subjects 1 and 2. The diameters and effective length of the ostia for the maxillary sinus are shown in Table VI. The resonance frequencies of the sinuses were numerically evaluated by implementing Eq. (7) and the proposed wall impedance Eq. (8) on the morphological data. The evaluated frequencies are also listed in Table VI. Comparing the resonance frequencies of the numerical computation with the measured results shown in Table V, both are consistent with one another within 10% error, except for a 28% error in the left side of the

maxillary sinus for Subject 1. The 28% error was probably caused by some changes in the morphology, which would occur, for example, if the ostium of the sinus was clogged with the mucosa since the two experiments were made at different times. This consistency provides a reasonable verification of the morphological and acoustical measurements.

B. Modeling the paranasal sinuses

Since the anti-resonance frequencies of the paranasal sinuses show strong individual differences and left-right asymmetry, it is not adequate to design a universal model to exactly represent all of the sinuses. For this reason, we propose an acoustical model for the paranasal sinuses based on a statistical analysis of our acoustical measurements and morphological data with reasonable simplifications.

Fig. 9 shows a histogram derived from the anti-resonance frequencies in Table V, where the ordinate is the number of zeros in each 100 Hz frequency band. In this figure, ten zeros out of 18 zeros fall into a range of 400 to 1000 Hz, while the remaining zeros are distributed in the region from 1 kHz to 2 kHz. For each subject, two or more zeros were located in the region below 1 kHz. This indicates that the effects of the paranasal sinuses are stronger in the lower frequency region. The distribution of zeros in Fig. 9 suggests that a four-zero model can approximate the acoustic characteristics of the paranasal sinuses: two zeros below 1 kHz and two zeros above 1 kHz. According to the distribution, the frequencies of the four zeros are proposed to be approximately 550 Hz, 750 Hz, 1300 Hz and 1700 Hz, respectively.

To model the four zeros, four Helmholtz resonators are employed and distributed among the three kinds of sinuses according to their degree of asymmetry. Here, the discussion about the left-right asymmetry is only focused on the volumes of the paranasal cavities, though the ostium dimension of the sinuses is also one of the factors causing asymmetry since there are no sufficient data on the ostia for the subjects. For this purpose, the left and right cavities of the paranasal sinuses are divided into two groups according to their size: large volume and small volume for the

subjects. A ratio of the large cavity to the small cavity is used to quantify the asymmetry. The ratios ranged from 1.02 to 1.18 for the maxillary sinus, from 1.17 to 1.41 for the frontal sinus, and from 1.34 to 2.33 for the sphenoidal sinus based on our MRI measurement (Dang et al., 1994). This result implies that the maxillary and frontal sinuses can be roughly considered to be symmetric between the left and right sides. Therefore, the maxillary and frontal sinuses are modeled using one resonator respectively, wherein the volumes of the two sinuses are defined as the sum of their left and right cavities. In contrast, the sphenoidal sinus has a relatively strong asymmetry. Taking this situation into account, the sphenoidal sinus is appropriately represented using two cavities: a large one and a small one, whose volumes are defined as the average values of the larger cavity group and smaller cavity group, respectively.

The four equivalent volumes corresponding to the paranasal sinuses are shown in Table VII. With reference to the measurements shown in Table V, the anti-resonance frequencies are approximately defined as 550 Hz for the maxillary sinus, 750 Hz for the frontal sinus, and 1300 Hz and 1700 Hz for the large cavity and small cavity, respectively, of the sphenoidal sinus. For the ostia of the sinuses, the dimensions were obtained by the MRI technique only for the maxillary sinus of two of our subjects. Fortunately, the anatomical data described in Section II give sufficient evidence for us to model the ostia. It should be noted that dimensions from the anatomical data are expected to be a little different from those for living subjects since the situation of nasal mucosa is different in both cases. The nasal mucosa usually lengthens the length and shortens the diameter of the ostia. Taking this into account, effective lengths of the ostia are proposed for the modeled sinuses with reference to the anatomical data and the MRI measurement, and shown in Table VII. From the given resonance frequencies and the geometric data in Table VII, the cross-sectional area of the throat is evaluated using Eq. (7) for each resonator, and also shown in the Table. Compared with the anatomical data, the cross-sectional area of the throat was realistic for each sinus. Realistic bandwidths were also obtained, which ranged from 108 to 216 Hz.

As a final step, these modeled sinuses are incorporated into a nasal tract model. In order to do so, their branch points in the nasal tract are set at 4.0, 5.0, and 6.5 cm from the nostrils, which correspond to the frontal, maxillary, and sphenoidal sinuses, respectively. The area function of the vocal tract for the nasal consonant /n/ was employed to simulate the effects of the paranasal cavities, which were obtained from volumetric MRI data in a previous study (Dang et al., 1994). A vocal tract wall impedance of $z_w = 1600 + j\omega 1.5$ was employed in this computation, which was proposed by Flanagan et al. (1975). Transfer functions from the vocal folds to the nostrils are obtained using the incorporated model, and shown in Fig. 10 for the nasal consonant. In the top curve without the sinuses, the two zeros at about 1200 and 4300 Hz were caused by the oral cavity branch, and the frequency of the first nasal formant was 420 Hz. When the larger cavity of the sphenoidal sinus is first incorporated (see the second curve from the top), a zero is introduced into the transfer function at 1320 Hz. The spectral shape around the zero is changed significantly, and the first formant is shifted down from 420 Hz to 390 Hz. As the resonators are incorporated one by one, the changes can be seen not only in the complexity of the transfer functions, but also in the formant frequencies and bandwidths. The effect of each sinus on the frequency and bandwidth of F1 is summarized in Table VIII. The maxillary sinus shows a stronger effect on the frequency of the first formant than the others, while the larger cavity of the sphenoidal sinus contributed more to the bandwidth. The results show that the paranasal sinuses not only add complexity, but also shape the nasal formants. The predicted frequency of the first nasal formant decreased from 422 to 301 Hz and the bandwidth increased from 85 to 103 Hz when all the sinuses were included.

VI. CONCLUSION

In the present study, a new method has been developed for acquiring the details of anti-resonance in vocal tract transmission characteristics using two-point sound pressures inside the vocal tract and at the radiating end. The anti-resonance frequency and branch point location of each resonator can be obtained by the spatial and spectral analysis of zero patterns. A pilot experiment on acoustic tubes of known

shapes showed that this method has an accuracy of about 2% error for the zeros and about 4% error for resonance peaks. The results also suggested that this method is capable of exploring the details of vocal tract transmission characteristics from short-period data of natural utterances.

The proposed method was used to investigate the acoustic characteristics of the paranasal sinuses. Measured anti-resonance frequencies were identified with corresponding sinuses by matching the branching location from the spatial analysis of zero patterns to that from volumetric MRI data for three subjects. The results showed that the three major paranasal sinuses: the sphenoidal, maxillary, and frontal sinuses, contribute zeros to the transmission characteristics of the nasal tract. The anti-resonance frequencies of the maxillary sinus were numerically verified by modeling the paranasal sinus as a Helmholtz resonator based on its morphological data. Both the measured and computed resonance frequencies were consistent with one another within 10% error except for one case where the error was 28%. Due to the complexities of the nasal cavity, however, it is difficult to give an appropriate explanation for every zero even if some of them appear in the region below 3 kHz. Such zeros can be seen at about 2300 Hz in the results for the left nasal passage for Subject 2, and at 2400 Hz and 2800 Hz in the results for the left and right nasal passages, respectively, for Subject 3. Some of them may derive from airy cells of the ethomoidal sinus. This could be verified by determining whether there is an appropriate relationship between its cavity volume and throat size.

The measured results of the paranasal cavity showed strong individual and asymmetric deference. To incorporate the paranasal sinuses into a vocal tract model, a four-zero model was proposed. Parameters of the Helmholtz resonators corresponding to the four-zero model were determined according to a statistical analysis of the acoustical results and the morphological data. Incorporating the model with the vocal tract area function of a nasal consonant, a realistic transfer function was obtained for the consonants. The results showed that the paranasal sinuses not only add complexity to the nasal spectra, but also shape the nasal formants.

ACKNOWLEDGMENTS

The authors would like to express their appreciation to Paul Milenkovic for his helpful comments about the measurement method. The authors would like to thank Hiroyuki Hirai and Naoki Kusakawa for their helpful discussions and help in the experimental setup. We are also grateful to Christine Shadle for her helpful comments on the early manuscript.

REFERENCES

Cassé, R., Kergomard, J., & Lurton, X. (1984). "Input impedance of brass musical instruments - comparison between experiment and numerical model," J. Acoust. Soc. Ame., 75, 1, 241-254.

Dang, J., Honda, K., and Suzuki, H. (1994). "Morphological and acoustical analysis of the nasal and the paranasal cavities," J. Acoust. Soc. Am. 96, 4, 2088-2100.

Dang, J. and Honda, K. (1995a). "An investigation of the acoustic characteristics of the paranasal cavities," Proc. of ICPhS95, Vol.1, 342-345 (Stockholm).

Dang, J. and Honda, K. (1995b). "A new method for measuring anti-resonance details of the vocal tract transmission characteristics, - an experimental study of acoustic tubes -," J. Acoust. Soc. Jpn(E), in press.

Davies, D., V. (1967). *Gray's anatomy*, 1279-1283 (Longmans, London), 34th Edition.

Donald, P. J. (1995). *Anatomy and Histology*. In P.J. Donald, J.L. Gluckman, and D.H. Rice (eds.), *The Sinuses*, (pp. 25-48). New York: Raven Press.

Fant, G. (1960). *Acoustic theory of speech production*, (Mouton, The Hague), p.139 (2nd ed., 1970).

Fant, G. (1980). "The relations between area functions and the acoustic signals," Phonetica, 37, 55-86.

Flanagan, J. L. (1972). Speech analysis synthesis and perception, Springer-Verlag, New York (2nd Edition).

Flanagan, J. L., Ishizaka, K., and Shipley, K. L. (1975). "Synthesis of speech from a dynamic model of the vocal cords and vocal tract," BST J., 54, 485-506.

Fujimura, O. and Lindqvist, J. (1964). "The sinewave response of the nasal tract," Q. prog. Status Rep., R. Inst. Tech., Stockh. 1, 5-10.

Fujimura, O. and Lindqvist, J. (1971). "Sweep-tone measurement of vocal-tract characteristics," J. Acoust. Soc. Am. 49, 2, 541-558.

Hattori, S., Yamamoto, K., and Fujimura, O. (1956). "Nasalization of vowels and nasals," Bull. of the Kobayashi Inst. of Res., 6, 226- 235(1956).

House, A. S. and Stevens, K. N. (1956). "Analog studies of the nasalization of vowels," J. Speech and Hearing Disorders, 21, 218- 232.

Imai, S., and Abe Y. (1979). "Spectral envelope extraction by improved cepstrum," IEICE, J62-A, 4, 217-228. (in Japanese).

Koyama, T. (1966). "Experimental study on the resonance of paranasal sinus," Journal Otolaryngology of Japan, 66, 1177-1191. (in Japanese).

Lindqvist-Gauffin, J, and Sundberg, J. (1976). "Acoustic properties of the nasal tract," Phonetica, 33, 161-168.

Lang J. (1989). *Clinical anatomy of the nose, nasal cavity & paranasal sinuses*, (New York: G Thieme Verlag), 62-69.

Maeda, S. (1982). "The role of the sinus cavities in the production of nasal vowels," in Proc. IEEE int. Conf. ASSP, 2, 911- 914.

Masuda, S. (1992) "Role of the maxillary sinus as a resonant cavity," Journal Otolaryngology of Japan, 95-70. (in Japanese).

Sondhi, M. M. and Schreoter, J. (1987). "A hybrid time-frequency domain articulatory speech synthesizer," IEEE Trans. ASSP-35, 7, 955-967.

Takeuchi, S., Kasuya, H. and Kido, K. (1977). "A study on the effects of nasal and paranasal cavities on the spectra of nasal sounds," J. Acoust. Soc. Jpn. 33, 4 163-172. (in Japanese).

Captions of tables and figures

Table I Anti-resonance frequencies of the paranasal cavities reported in previous studies. (Values given in Hz)

Table II Geometries of the tubes used in the pilot experiment.

Table III Distance measured from the nostrils to the openings of the paranasal sinuses and to the posterior nares. (Unit: cm)(Unit: cm)

Table IV Speech material used in this experiment.

Table V Anti-resonance frequencies of the paranasal sinuses estimated from acoustic measurements. (Hz)

Table VI Resonance frequencies (F) of the maxillary sinus calculated from morphological data.(V: Volume of the cavity; A: Cross-sectional area of the ostium; L: Length of the ostium.)

Table VII Modeled paranasal sinuses. Equivalent volumes and effective length of the throat are given based on the volumetric MRI data. Resonance frequencies are based on the acoustic measurements. The cross-sectional areas of the throat are computed using Eq. (7).

Table VIII The effect of the modeled sinuses on frequency (F1) and bandwidth (B1) of the first formant. (Fz is the frequency of the zero caused by the sinuses)

Fig. 1 Sketch of an acoustical tube with a branch. Chain matrices K_2 and K_1 cover tube segments of x_i to x_b and x_b to x_e, respectively. K_b is a matrix coupling the branch to the main tube.

Fig. 2 Schematic diagram of the system for measuring transmission characteristics of a tube segment from the measurement point to the radiation end.

Fig. 3 Transmission characteristics obtained from (a) a uniform tube and (b) a tube with branches using a sweeptone sound source. (The length of each measurement segment is shown on the right side of each graph. The dashed lines indicate the zeros caused by a 25.5-cm-long branch. The arrow shows the zero caused by a 3.4-cm-long branch.)

Fig. 4 Anatomical structure of the nasal and paranasal cavities.

(a) Projection of 3D reconstruction from volumetric MRI data showing the nasal cavity and the four paranasal sinuses.

(b) Locations of the major paranasal sinuses are outlined by dashed lines, and their openings are indicated by a solid ellipse with an arrow. (The turbinates are removed to expose the middle meatus.)

Fig. 5 A schematic diagram of the setup for measuring the acoustic characteristics of the paranasal cavities.

Fig. 6 Transmission characteristics obtained from each measurement segment for Subject 1, (a) for the left side of the nasal tract and (b) for the right side. (The length of the measurement segment is shown on the right side of each column. The white arrows indicate the zeros caused by the frontal sinus, the black arrows are for the maxillary sinus, and the V-shaped arrows are for the sphenoidal sinus.)

Fig. 7 Transmission characteristics obtained from each measurement segment for Subject 2, (a) for the left side of the nasal tract and (b) for the right side. (The length of the measurement segment is shown on the right side of each column. The white arrows indicate the zeros caused by the frontal sinus, the black arrows are for the maxillary sinus and the V-shaped arrows are for the sphenoidal sinus.)

Fig. 8 Transmission characteristics obtained from each measurement segment for Subject 3, (a) for the left side of the nasal tract and (b)

for the right side. (The length of the measurement segment is shown on the right side of each column. The white arrows indicate the zeros caused by the frontal sinus, the black arrows are for the maxillary sinus and the V-shaped arrows are for the sphenoidal sinus.)

Fig. 9 Number of zeros in each 100 Hz band, obtained by acoustic measurements for all three subjects as described in Section IV.

Fig. 10 Transfer functions from the glottis to the nostrils obtained when incorporating the sinuses one by one with area function of nasal consonant /n/. (SS(L) and SS(S) are the large and small cavities of the sphenoidal sinus, MS is the maxillary sinus and FS is the frontal sinus.)

Table I Anti-resonance frequencies of the paranasal cavities reported in previous studies. (Values given in Hz)

Researchers (Date)	Sphenoidal sinus	Maxillary sinus	Frontal sinus
Koyama (1966)	500～1200	400～1000	-
Lindqvist et al.(1971)	-	200～800	1000 ～ 2000
Takeuchi et al.(1977)	～1500	300～400	～1000
Maeda (1982)	-	450	-
Masuda (1992)	-	1000～2000	-

Table II Geometries of the tubes used in the pilot experiment. (Unit: cm)

	Main tubes		Branch 1			Branch 2		
Tubes	Leng.	Diam.	Dist.	Leng.	Diam.	Dist.	Leng.	Diam.
Tube A	21.0	2.0	-	-	-	-	-	-
Tube B	19.0	2.2	6.5	22.5	1.2	12.5	3.4	1.6

*Leng.: Length; Diam.: Diameter;
Dist.: Distance from branch point to radiating end of the main tubes.

Table III Distance measured from the nostrils to the openings of the paranasal sinuses and to the posterior nares. (Unit: cm)

Subjects	Sphenoidal S.	Maxillary S.	Frontal S.	Posterior nares
Subj.1	6.2	5.1	4.3	7.6
Subj.2	6.0	4.3	4.0	7.3
Subj.3	6.8	4.3	4.0	7.5

Table IV Speech material used in this experiment.

Nasal consonants	NV syllables
/m/	/ma/, /mi/, /mu/, /me/, /mo/
/n/	/na/, /ni/, /nu/, /ne/, /no/

Table V Anti-resonance frequencies of the paranasal sinuses estimated from acoustic measurements. (Hz)

	Sphenoidal S.		Maxillary S.		Frontal S.	
Subjects	Left	Right	Left	Right	Left	Right
Subj.1	1350	750	1100	890	630	2060
Subj.2	1900	1750	630	580	?	1450
Subj.3	930	1700	530	510(400)	1160	740

Table VI Resonance frequencies (F) of the maxillary sinus calculated from morphological data.(V: Volume of the cavity; A: Cross-sectional area of the ostium; L: Length of the ostium.)

	Left side				Right side			
	$V(cm^3)$	$A(cm^2)$	L(cm)	F(Hz)	$V(cm^3)$	$A(cm^2)$	L(cm)	F(Hz)
Subj. 1	11.0	0.099	0.46	786	9.9	0.086	0.38	850
Subj. 2	16.1	0.076	0.45	575	16.5	0.065	0.43	538

Table VII Modeled paranasal sinuses. Equivalent volumes and effective length of the throat are given based on the volumetric MRI data. Resonance frequencies are based on the acoustic measurements. The cross-sectional areas of the throat are computed using Eq. (7).

	S.S.(L)	S.S.(S)	M.S.	F. S.
Volume (cm^3)	11.3	6.8	33	6.2
Length (cm)	0.30	0.30	0.45	1.0
Area (cm^2)	0.185	0.185	0.145	0.11
f_r (Hz)	1305	1682	552	749
B (Hz)	188	216	108	124

*S.S.(L) and S.S.(S) represent the large and small cavities of the sphenoidal sinus, respectively.

Table VIII The effect of the modeled sinuses on frequency (F1) and bandwidth (B1) of the first formant. (Fz is the frequency of the zero caused by the sinuses)

	S.S.(L)	S.S.(S)	M.S.	F. S.
Fz (Hz)	1305	1685	552	749
ΔF1 (Hz)	-27	-15	-72	-7
ΔB1 (Hz)	8	6	1	3

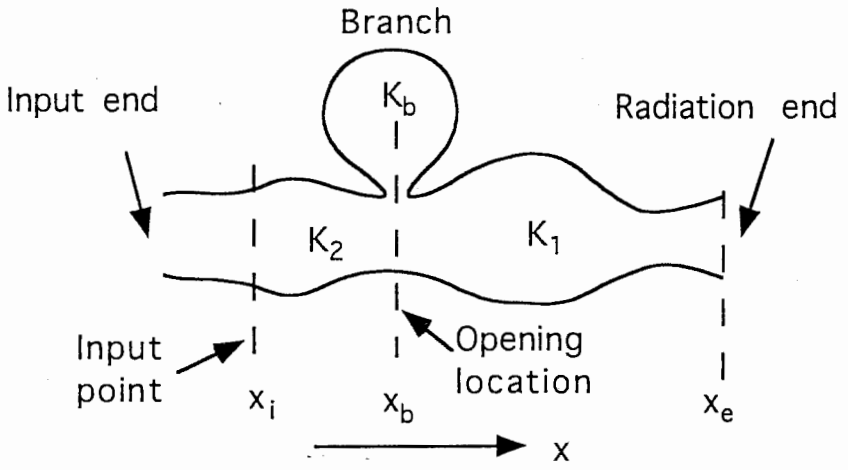

Fig. 1 Sketch of an acoustical tube with a branch. Chain matrices K_2 and K_1 cover tube segments of x_i to x_b and x_b to x_e, respectively. K_b is a matrix coupling the branch to the main tube.

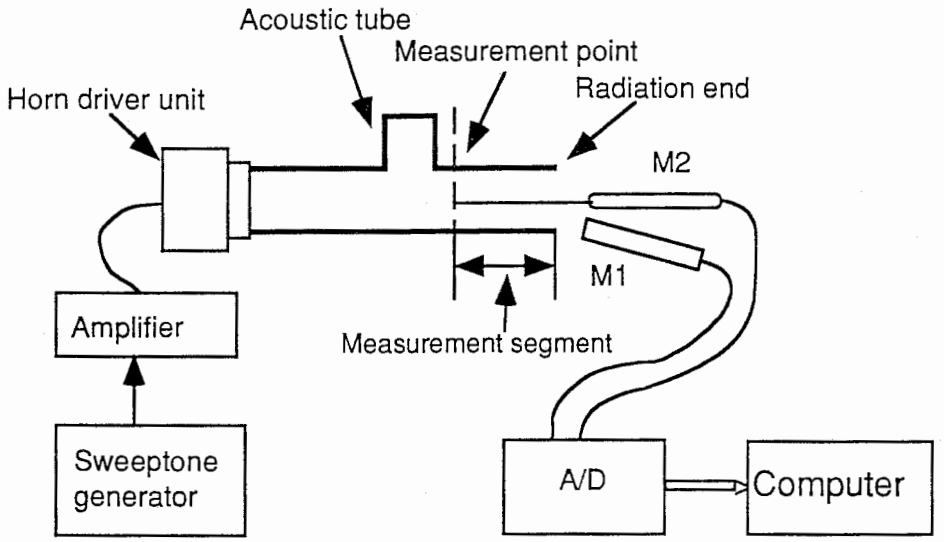

Fig. 2 Schematic diagram of the system for measuring transmission characteristics of a tube segment from the measurement point to the radiation end.

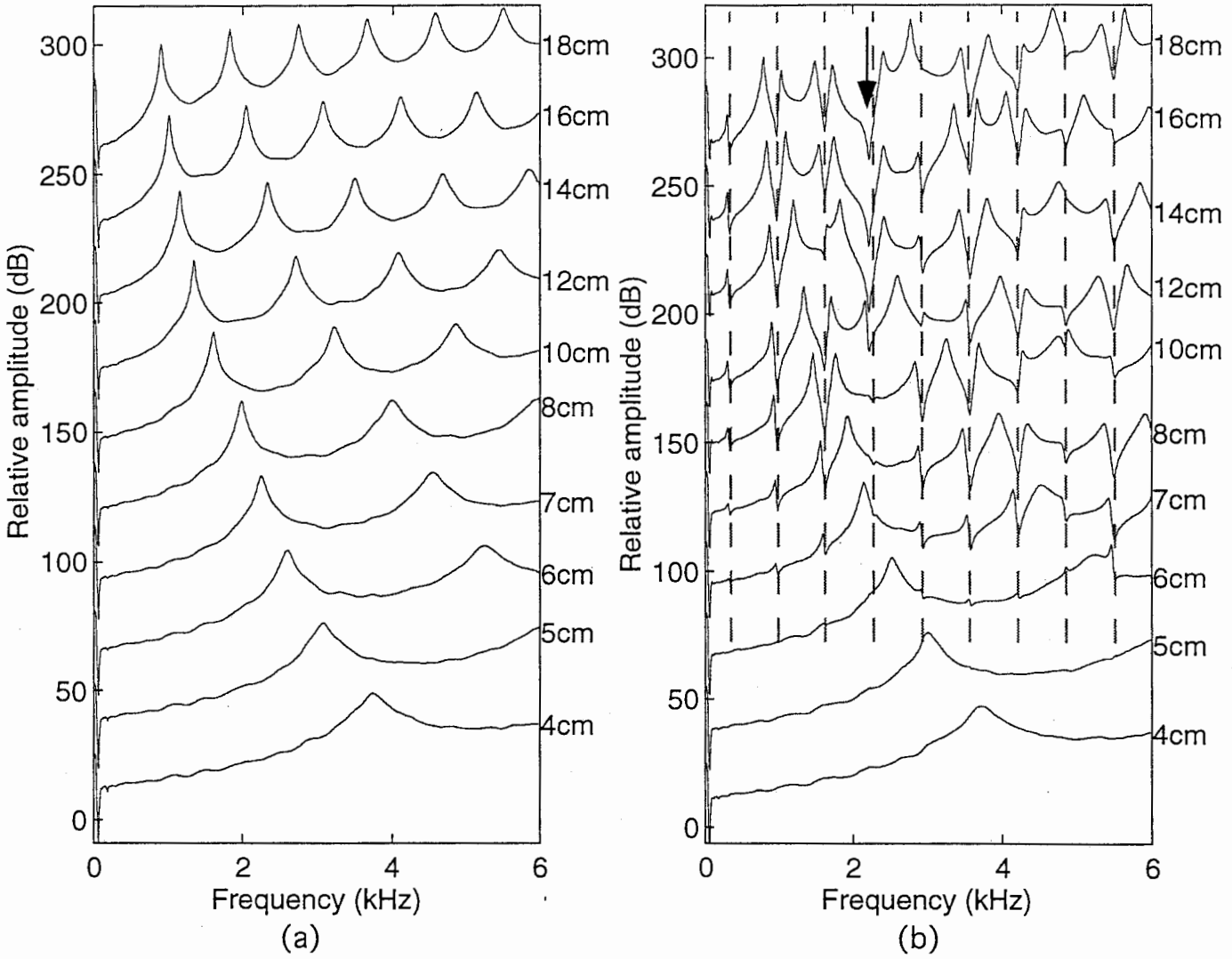

Fig. 3 Transmission characteristics obtained from (a) a uniform tube and (b) a tube with branches using a sweeptone sound source. (The length of each measurement segment is shown on the right side of each graph. The dashed lines indicate the zeros caused by a 25.5-cm-long branch. The arrow shows the zero caused by a 3.4-cm-long branch.)

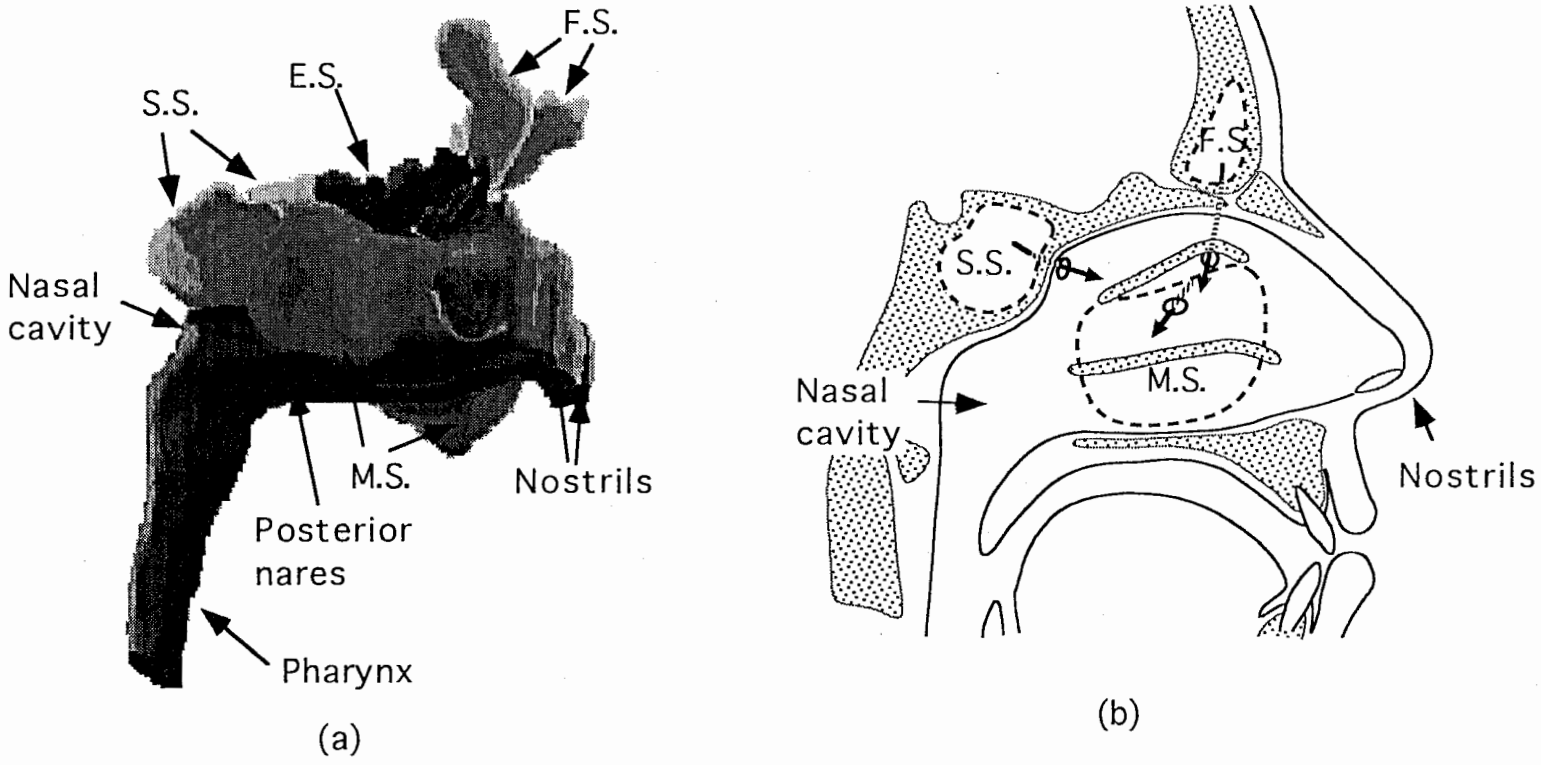

Fig. 4 Anatomical structure of the nasal and paranasal cavities.
(a) Projection of 3D reconstruction from volumetric MRI data showing the nasal cavity and the four paranasal sinuses.
(b) Locations of the major paranasal sinuses are outlined by dashed lines, and their openings are indicated by a solid ellipse with an arrow. (The turbinates are removed to expose the middle meatus.)

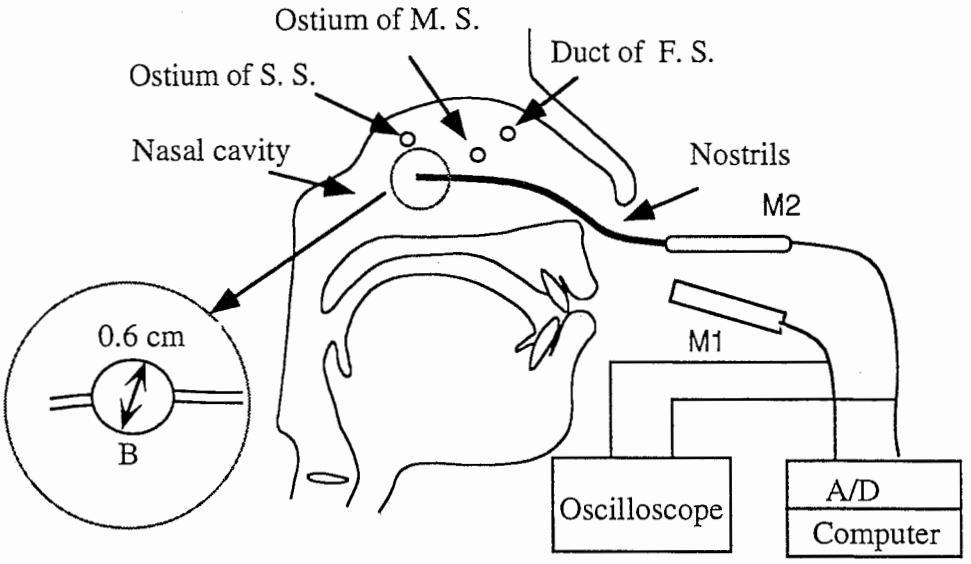

Fig. 5 A schematic diagram of the setup for measuring the acoustic characteristics of the paranasal cavities.

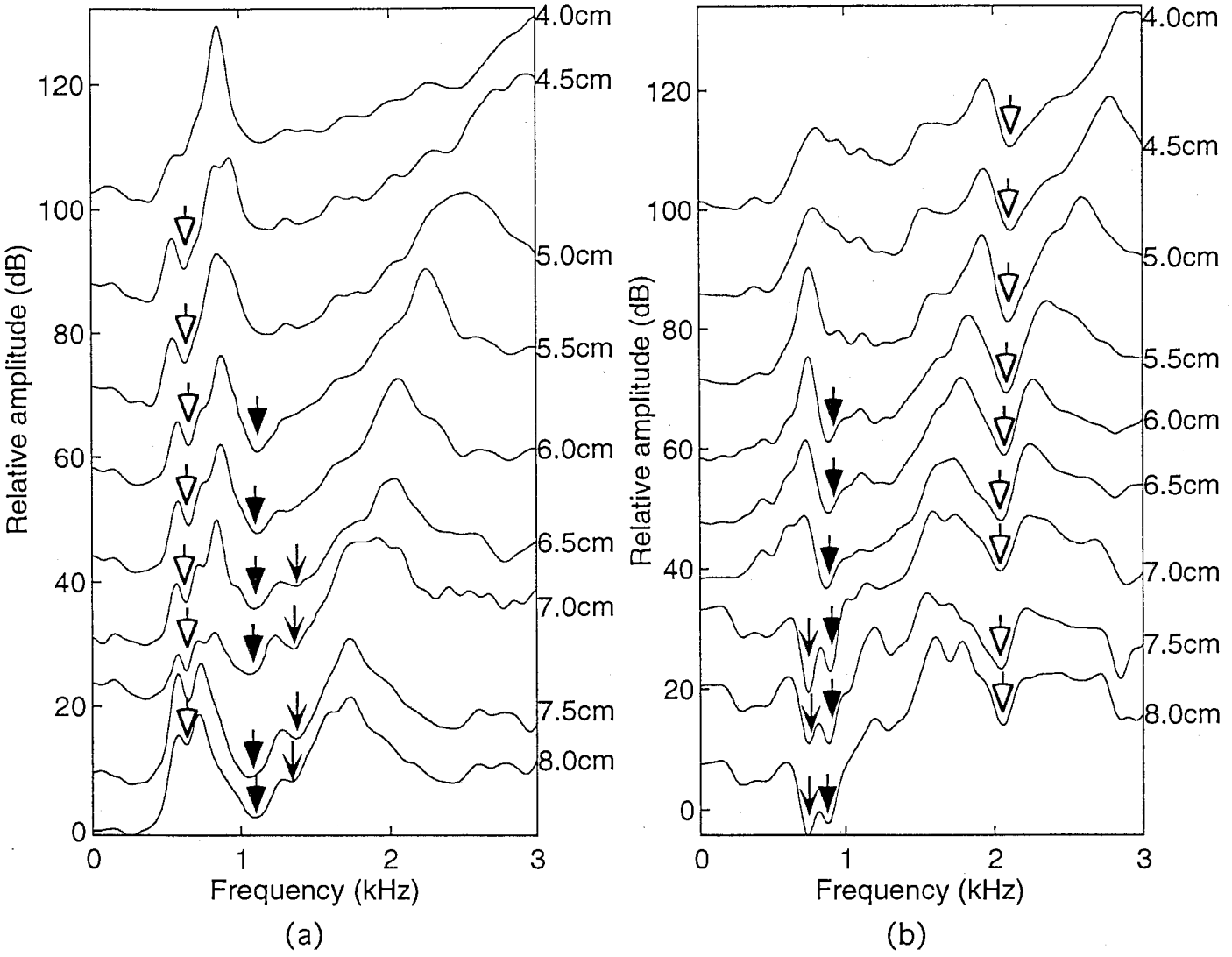

Fig. 6 Transmission characteristics obtained from each measurement segment for Subject 1, (a) for the left side of the nasal tract and (b) for the right side. (The length of the measurement segment is shown on the right side of each column. The white arrows indicate the zeros caused by the frontal sinus, the black arrows are for the maxillary sinus, and the V-shaped arrows are for the sphenoidal sinus.)

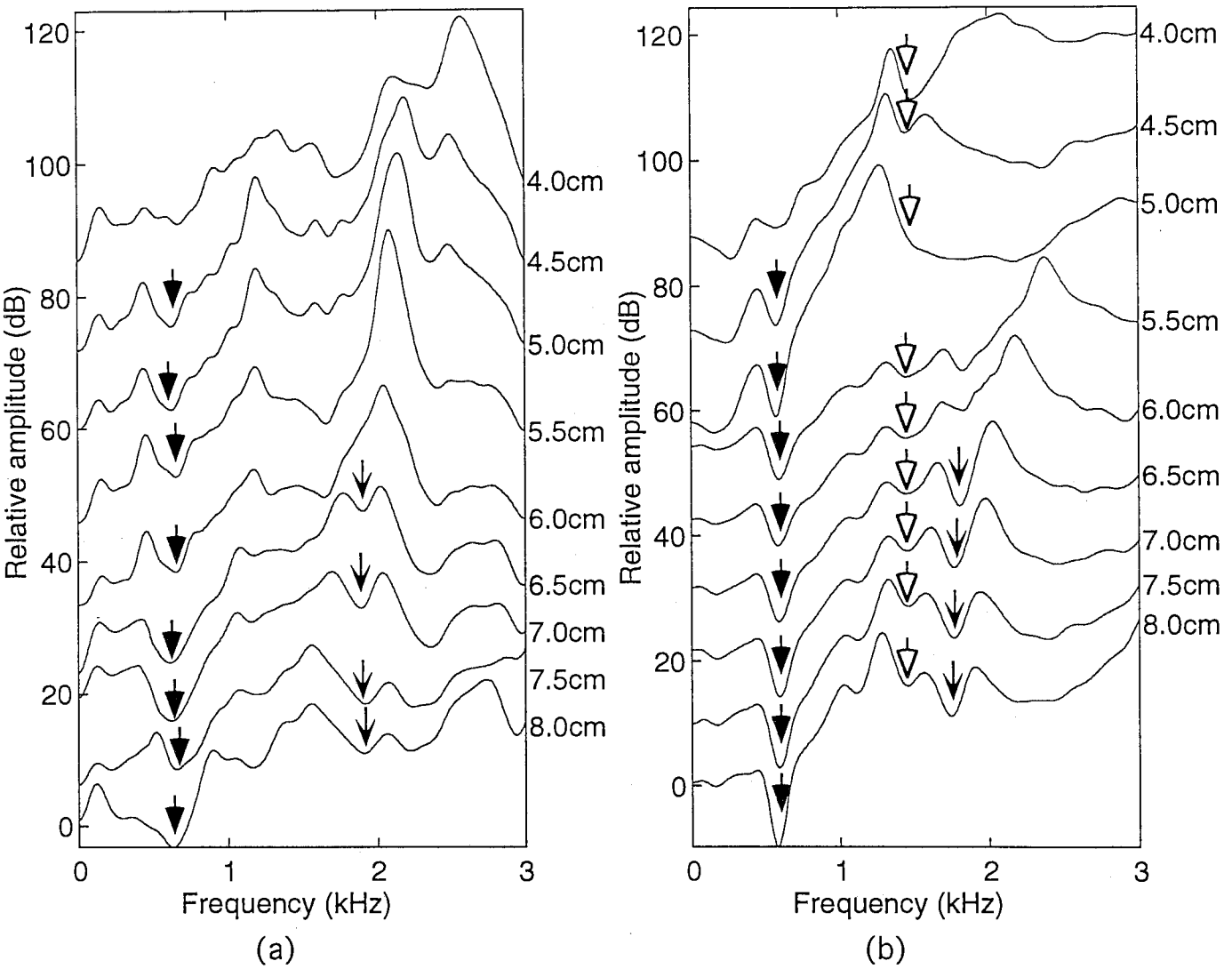

Fig. 7 Transmission characteristics obtained from each measurement segment for Subject 2, (a) for the left side of the nasal tract and (b) for the right side. (The length of the measurement segment is shown on the right side of each column. The white arrows indicate the zeros caused by the frontal sinus, the black arrows are for the maxillary sinus and the V-shaped arrows are for the sphenoidal sinus.)

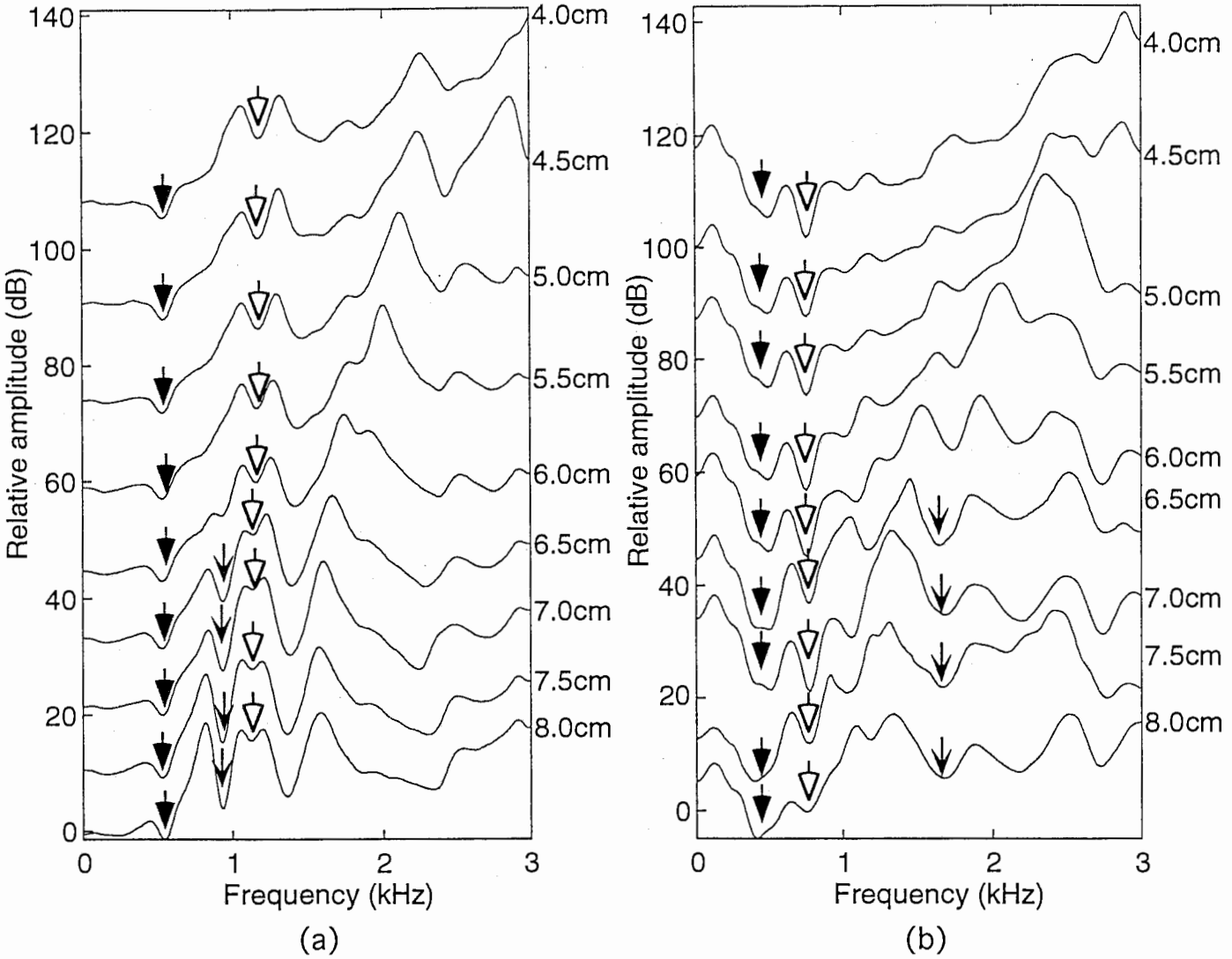

Fig. 8 Transmission characteristics obtained from each measurement segment for Subject 3, (a) for the left side of the nasal tract and (b) for the right side. (The length of the measurement segment is shown on the right side of each column. The white arrows indicate the zeros caused by the frontal sinus, the black arrows are for the maxillary sinus and the V-shaped arrows are for the sphenoidal sinus.)

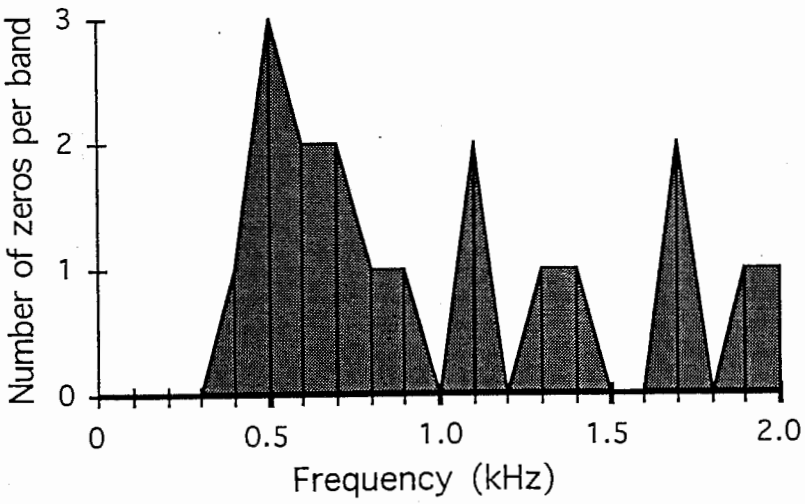

Fig. 9 Number of zeros in each 100 Hz band, obtained by acoustic measurements for all three subjects as described in Section IV.

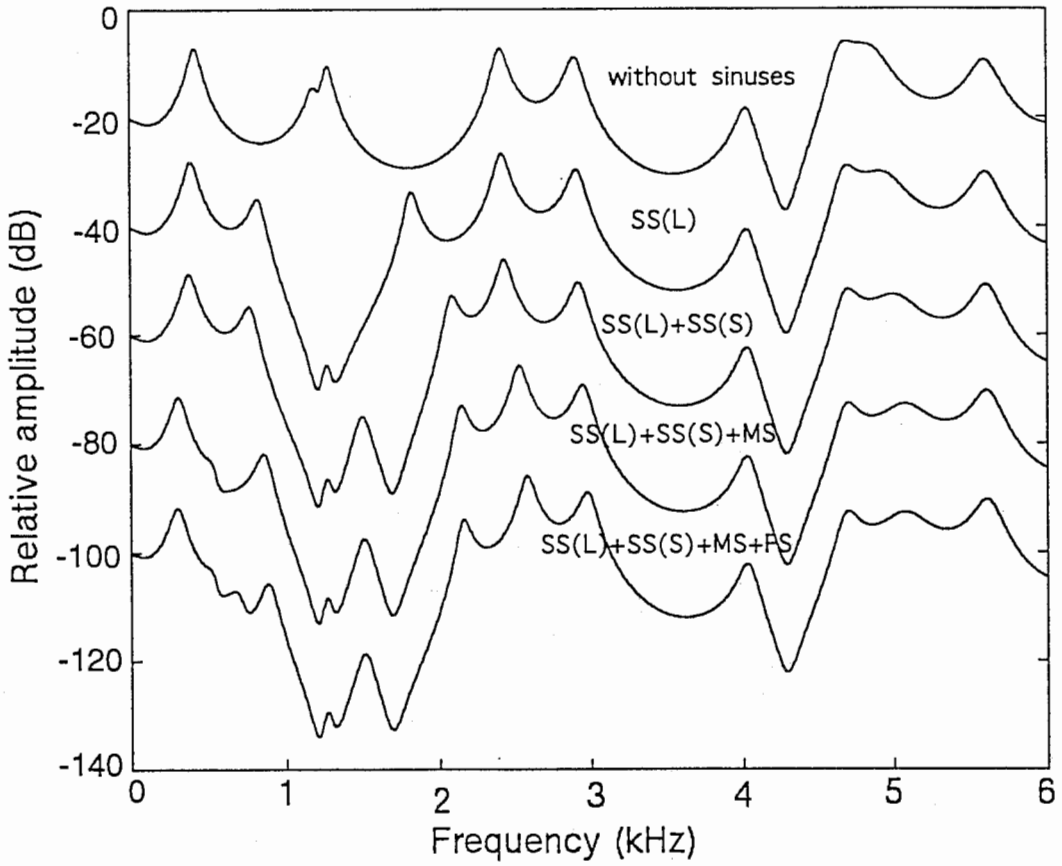

Fig. 10 Transfer functions from the glottis to the nostrils obtained when incorporating the sinuses one by one with area function of nasal consonant /n/. (SS(L) and SS(S) are the large and small cavities of the sphenoidal sinus, MS is the maxillary sinus and FS is the frontal sinus.)